Journal of Power Sources 195 (2010) 6031–6036

Contents lists available at ScienceDirect

Journal of Power Sources

journal homepage: www.elsevier.com/locate/jpowsour

Si–graphite composites as anode materials for lithium secondary batteries

Yong Nam Jo[a], Yeri Kim[a], Jeom Soo Kim[a], Jun Ho Song[a], Ki Jae Kim[a], Chong Yun Kwag[b], Dong Jun Lee[b], Chul Wan Park[b], Young Jun Kim[a,*]

[a] Advanced Batteries Research Center, Korea Electronic Technology Institute, Seongnam 463-816, Republic of Korea
[b] SODIFF Advanced Materials Co., Ltd., Yeongju 750-080, Republic of Korea

ARTICLE INFO

Article history:
Received 23 December 2009
Received in revised form 2 March 2010
Accepted 3 March 2010
Available online 11 March 2010

Keywords:
Lithium secondary battery
Anode materials
Silicon
Silicon–graphite composites
High capacity

ABSTRACT

Two types of Si–graphite (Si–C) composites are synthesized and evaluated for anode materials of lithium secondary batteries. The mechano-chemical milling and the rotational impact blending methods are applied to synthesize two types of Si–C composites. Graphite powders having Si on the surface (type A) is synthesized by mechano-chemical milling using the pitch as a binder. Si embedded inside the graphite particle (type B) is synthesized by rotational impact blending. The loading level of Si is about 20 wt% for both type Si–C composites. The location of Si is verified by observing cross sectional images of particle and conducting EDS mapping. The initial discharge capacity of type B has larger value than that of type A, while the type A shows better cycle performance than type B. The efficiency of first cycle is about 87% for both types A and B.

1. Introduction

Si has been projected as a candidate for anode material in lithium secondary batteries because of its high theoretical capacity (4200 mAh g^{-1}). Even though it has much higher theoretical capacity than the graphite (372 mAh g^{-1}), there are many obstacles to be commercialized. The major problems are the volume change (expansion/contraction) during the alloying (charge) and de-alloying (discharge) reaction with Li^+ ions (420%) and the low electrical conductivity [1–5]. Due to the volume change, Si particles are isolated from electron conducting paths in the electrode resulted to lose Li^+ storage ability eventually. To resolve this problem, different types of approach has been investigated such as reducing particle size to nano-level [6,7], dispersing Si in other materials matrix [8–13], and fabricating Si in the form of thin films [14–17]. Carbon materials are used common matrix because of its effect on increasing the electrical conductivity, reducing the volume change, and contributing the cell capacity [18–20].

In this paper, we report the characteristics of two different types of Si–C composites including the preparation, morphology verification, and electrochemical performance. One is Si particles placed on the graphite surface (type A) and the other is Si particles embedded in the graphite (type B).

2. Experimental

2.1. Sample preparation

The Si–C composites were made from natural flake graphite (FG) and Si particles (Sigma–Aldrich, 325 mesh). The average diameter of FG particle was 200 μm and overall particle shape was thin and flat. Si powder was ball-milled to reduce the size down to 100 nm. The morphologies of FG and Si are shown in Fig. 1. For the type A, spherical graphite (SG) was prepared by shape modification method using rotational impact blending machine, which was useful method to synthesize spherical graphite having high tap density and low surface area [21]. The mixture of SG, Si, and pitch (6:2:2 by weight ratio) was treated by mechano-chemical milling to produce Si coated graphite powder. The pitch was used as a binder. The resulting material was heated at 900 °C under N_2 atmosphere for 1 h. The type B Si–C was synthesized using the mixture of FG and Si (8:2 weight ratio) by shape modification method. The pitch (5 wt%) was added to resulted material during the heat treatment at 900 °C under N_2 for 1 h.

2.2. Materials characterization

The cross section of Si–C composites was prepared using JEOL SM-09010 cross section polisher (CP). FEI™ Qunta 3D FEG was used for the examination of cross sectional images of Si–C composites. Samples for investigation were coated by Pt to protect the morphology while Ga^+ is induced. The images of raw materials and Si–C

* Corresponding author. Tel.: +82 31 789 7490; fax: +82 31 789 7499.
E-mail address: yjkim@keti.re.kr (Y.J. Kim).

0378-7753/$ – see front matter © 2010 Elsevier B.V. All rights reserved.
doi:10.1016/j.jpowsour.2010.03.008

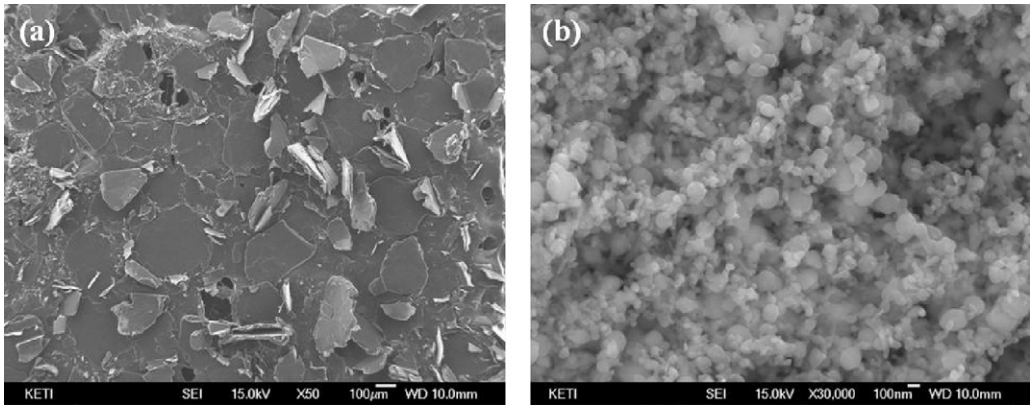

Fig. 1. The FE-SEM images of natural flake graphite and Si.

composites were examined using a JEOL JSM-7000F field-emission scanning electron microscope (FE-SEM). The elemental analysis of Si–C was characterized by Oxford Inca (EDS) attached FE-SEM. The phase of product powder was identified by Rigaku D-MAX2500-PC X-ray diffractometer (XRD) using Cu Kα radiation. The contents of Si in Si–C composites were estimated by using TA instrument SDT Q600 thermal gravimetric analysis (TGA).

2.3. Electrochemical characterization

Electrodes were fabricated by intimately mixing the active Si–C power, corresponding to 96% by weight of total electrode, with 2% stydiene-butadiene-rubber (SBR, BM-400B, Zeon, 40% emulsion in water) and 2% sodium carbomethyl cellulose (CMC, BSH12, DAI-ICHI Kogyo Seiyaku) in distilled water. The electrode slurry was spread on a copper foil (as a current collector, 10 μm thickness) using a doctor blade. The electrode was roll-pressed in order to enhance the inter-particle contact and to ensure a better adhesion to the current collector. The electrodes were subsequently dried under vacuum at 120 °C for 12 h. Then the electrode were punched into disk (∅ = 12 mm). The material loading was 7 mg cm^{-2} (including conducting agent and binder) with a thickness of 70 μm (excluding Cu foil).

Beaker-type two electrode cells were fabricated for the electrochemical measurements with lithium foil counter and an electrolyte consisting of a 1 M $LiPF_6$ solution in ethylene carbonate (EC):ethylmethyl carbonate (EMC) (1:2 by volume) containing vinyl carbonate (VC, 1 wt%) as an additive. All the cell assembly was carried out in dry room which dew point was controlled less than −45 °C. A porous polyethylene membrane was used as the separator. Cells were charged (lithiated) and discharged (delithiated) at constant current (140 mA g^{-1}) followed by constant voltage (only

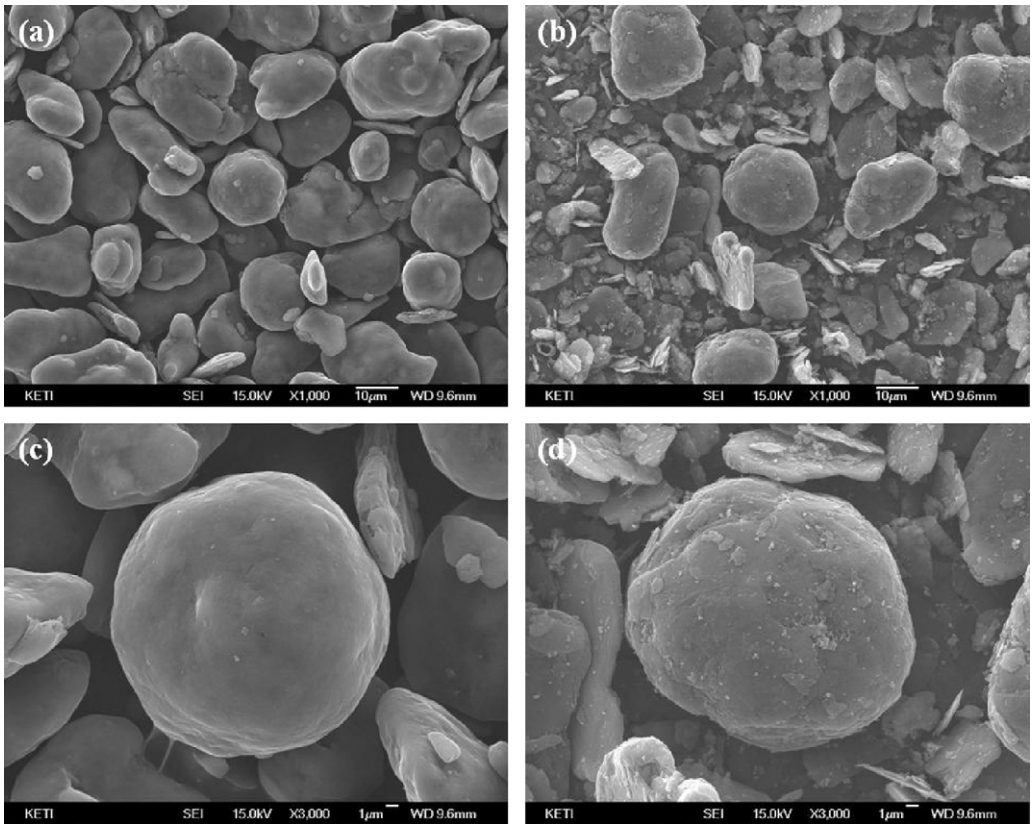

Fig. 2. The FE-SEM images of Si–C composites. (a) Type A (X1,000); (b) type B (X1,000); (c) type A (X3,000); (d) type B (X3,000).

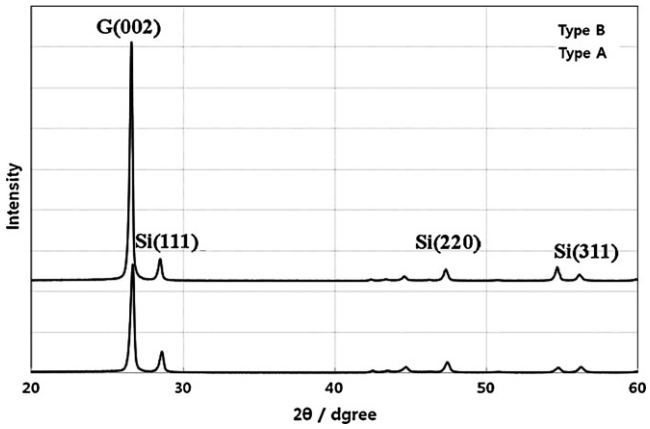

Fig. 3. The XRD patterns of Si–C composites. Note that G denotes graphite.

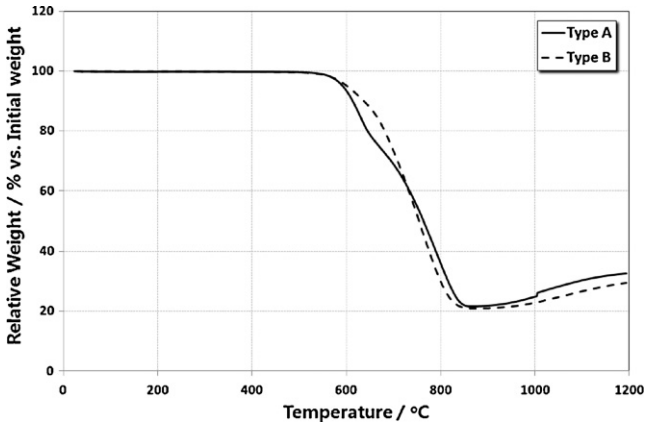

Fig. 4. The TGA analysis of Si–C composites. Note that the solid line denotes type A, dashed line type B.

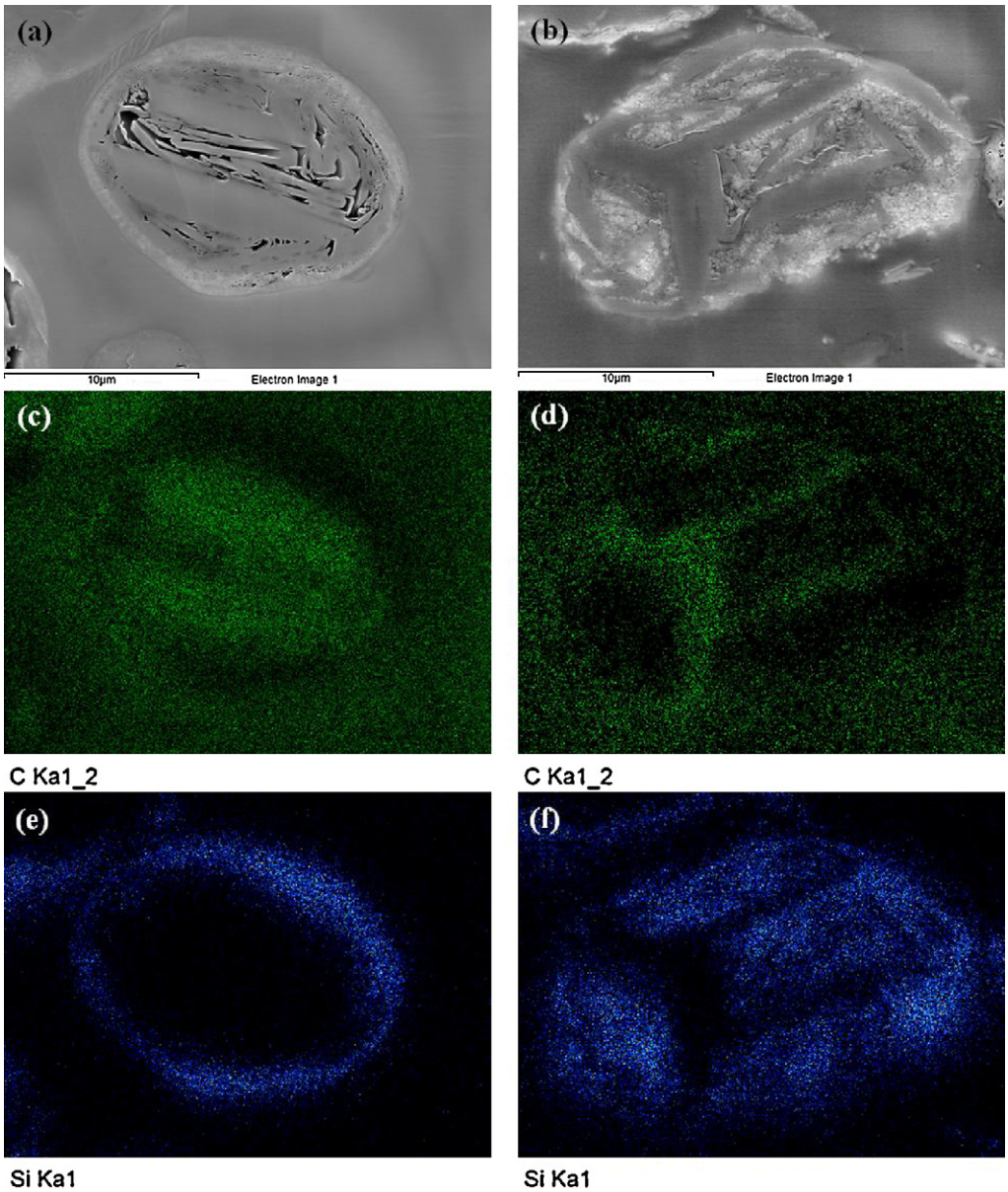

Fig. 5. The EDS mapping of cross sectional Si–C composites. (a) Cross sectional FE-SEM image of type A; (b) type B; (c) C element EDS mapping in type A; (d) C element EDS mapping in type B; (e) Si element EDS mapping in type A; (f) Si element EDS mapping in type B.

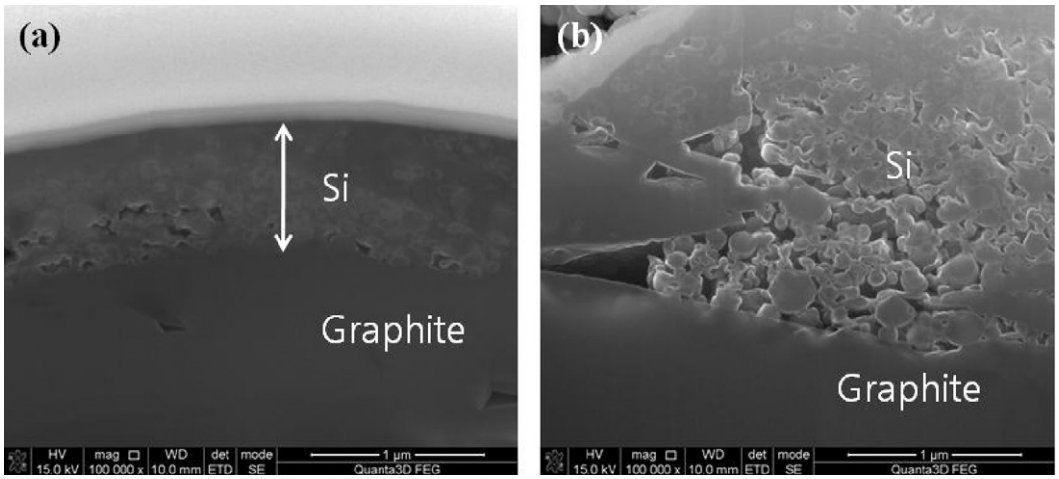

Fig. 6. The FIB cross sectional images of Si–C composites. (a) Type A; (b) type B.

applied during charging, 0.008 V for the limit of 35 mA g^{-1}) between voltage limits that were programmed to vary between 0.008 and 1.5 V (*vs.* Li/Li^+). The electrochemical measurements were carried with a TOSCAT-3100U battery cycler (Toyo System Co.) at ambient temperature.

3. Results and discussion

The powder morphology of Si–C composites is shown in Fig. 2. Type A has rounded shape while type B has mixed shapes of flake and round. The average size of rounded particle is about 15 μm. The enlarged surface images of types A and B (Fig. 2c and d) shows quite different morphologies which the type A has a smooth surface while the type B has a rough one. Different morphology is attributed to synthesis methods applied to type A and type B. For type A, the rounded shape graphite was coated with Si powders and pitch. Meanwhile, type B was prepared by pitch coating after the shape modification process by mixing of flaky shape graphite and Si powders. Some flaky shapes observed in type B indicates that the modification process was not effective enough to convert flaky shape to rounded shape.) and after 30 cycles (Fig. 11

The XRD patterns of Si–C composites are shown in Fig. 3. Only Si and graphite phases were observed in both types A and B. In type B, the relative intensity ratio (10.77) of graphite (0 0 2) peak to the Si(1 1 1) is higher than that of type A (5.06). This can be attributed to the high Si concentration exposed on the surface of type A. The amount of Si was estimated by TGA analysis on Si–C composites as shown in Fig. 4. The graphite was oxidized to CO_2 in the range of 550–820 °C resulting the weight loss while Si was not oxidized. In the range of 820–1200 °C, remained Si was oxidized and the weight of sample increased [18]. The estimated portion of Si in types A and B were 21.5 wt% and 20.8 wt%, respectively. The different curve shape of both type Si–C composites was originated from the higher content of pitch in type A. As for the sample type A, pitch was used as a binder to prepare Si–C composite. It could be carbonized to soft carbon under 900 °C heat treatment. Under air atmosphere,

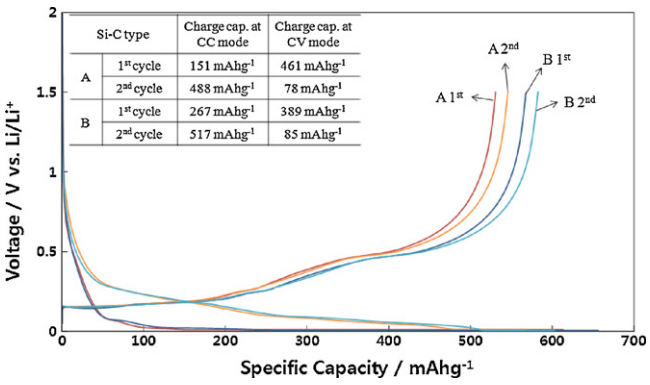

Fig. 7. The galvanostatic voltage profiles of Si–C composites during the first and second cycle.

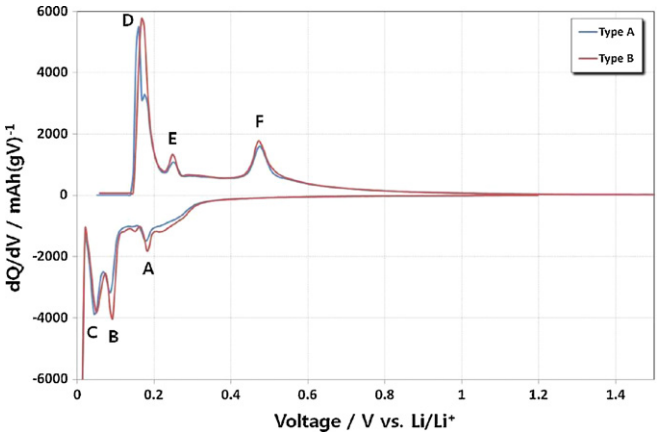

Fig. 8. The differential capacity plots of Si–C composites.

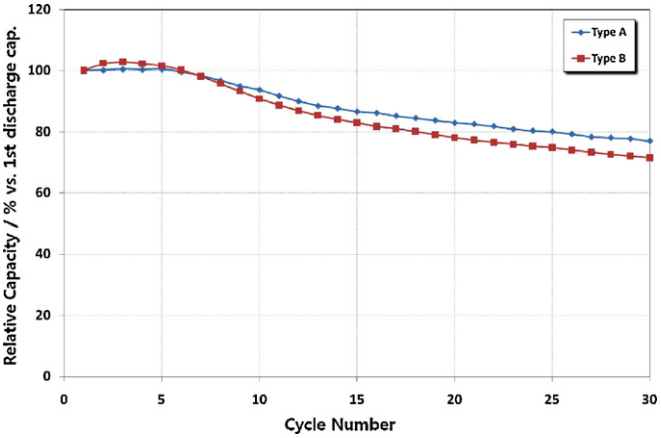

Fig. 9. Cycle performances of types A and B.

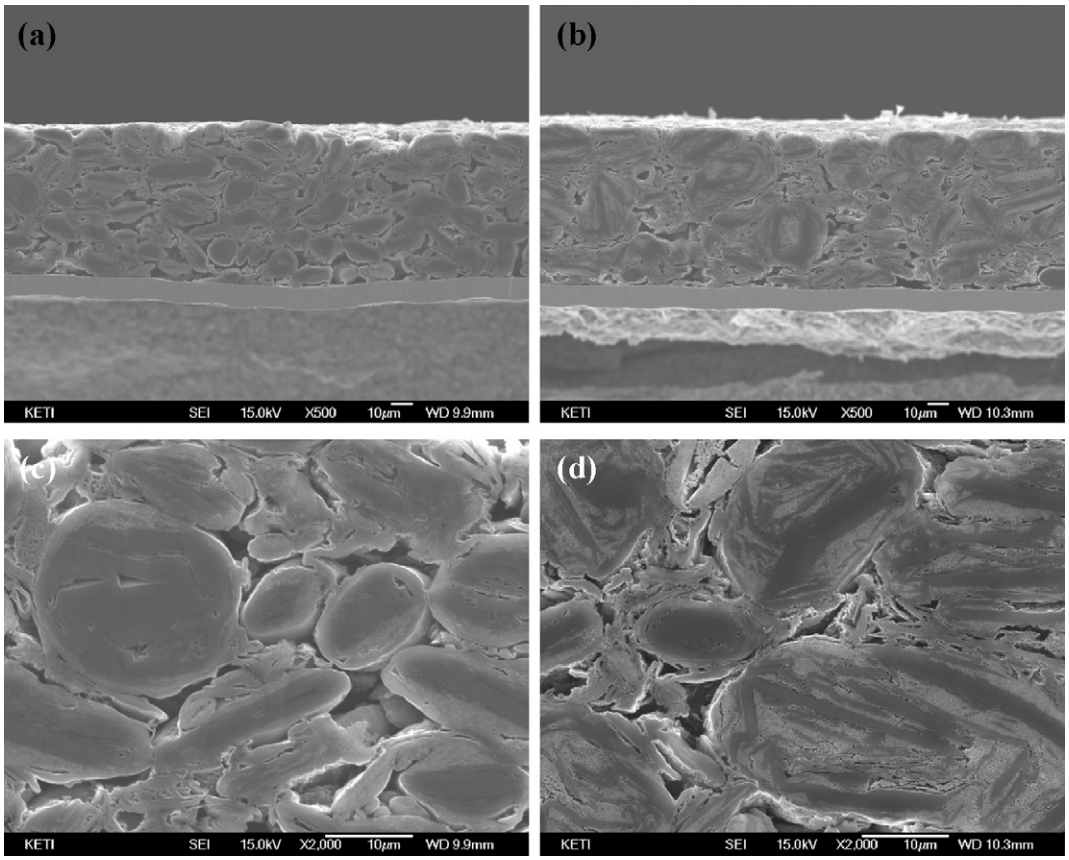

Fig. 10. The cross sectional FE-SEM images of pristine Si–C electrodes. (a) Type A (X500); (b) type B (X500); (c) type A (X2,000); (d) type B (X2,000).

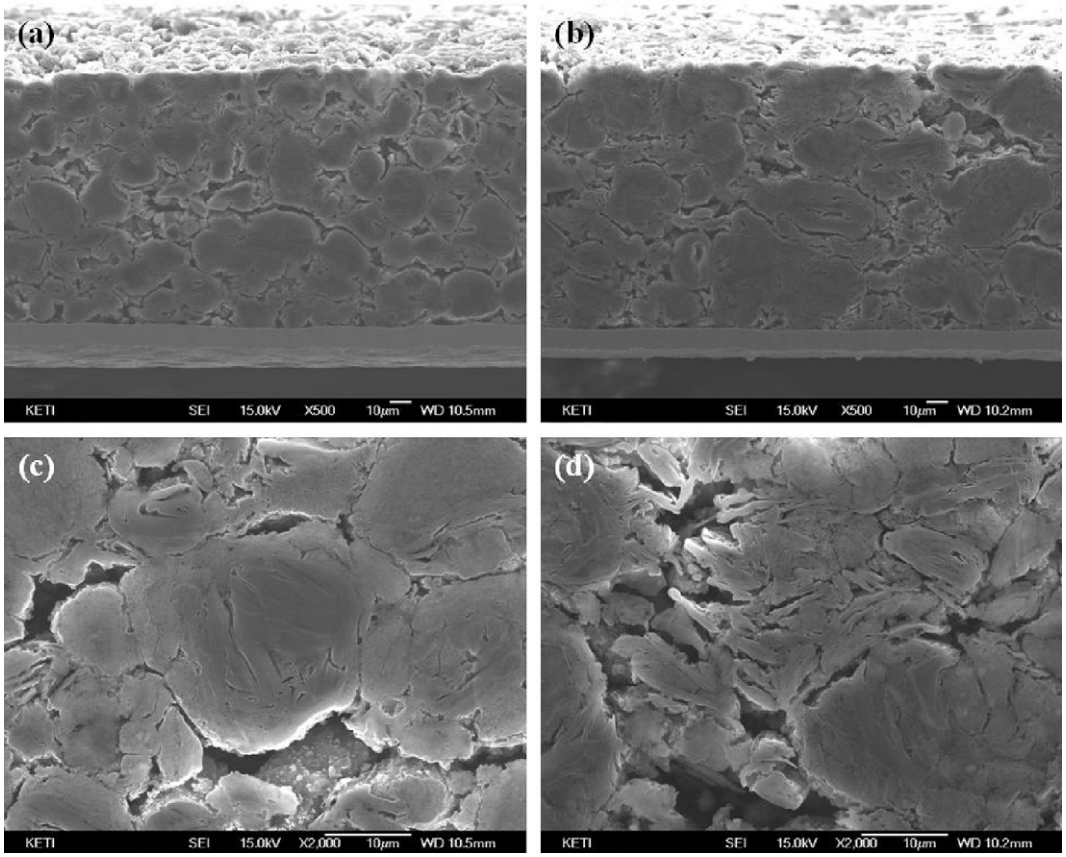

Fig. 11. The cross sectional FE-SEM images of Si–C electrodes after 30 cycles. (a) Type A (X500); (b) type B (X500); (c) type A (X2,000); (d) type B (X2,000).

the soft carbon can be easily oxidized to CO_2 gas at earlier temperature compared with graphite. As a result, the S-shape curve was obtained in TGA analysis.

Fig. 5 shows the cross sectional FE-SEM images of Si–C composites and EDS mapping results. The samples were prepared with ion beam polisher using Ar^+ ion as an ion source. It is clearly observed that the Si is located outside of particles in type A while the Si is placed inside the particles in type B. For further investigation, cross sectional images of Si–C composites were examined by using FIB as shown in Fig. 6. Si particles were coated on the graphite surfaces with ~1 μm thickness in type A (Fig. 6a) while Si particles were embedded in the empty volume of graphite in type B (Fig. 6b).

The electrochemical properties of Si–C composites were studied by applying the constant current–constant voltage (CC–CV) cycle technique (Fig. 7). Type A shows the capacities of 613 mAh g^{-1} for charge and 530 mAh g^{-1} for discharge, respectively.

In type B, both charge (657 mAh g^{-1}) and discharge (568 mAh g^{-1}) capacities are higher than type A. Both types A and B have coulombic efficiencies of 86.4%. The voltage profiles of types A and B are very close to each other indicating that the resistance of graphite is not affected by Si coating. Type A has smaller specific capacity than type B has. One possible reason to explain this result is the electrical isolation of graphite which does not contribute to electrode capacity. It is well known that Si goes with severe volume change when it reacts with lithium during electrochemical cycling. The volume change of coated Si on graphite losing contact between Si and graphite due to the volume change of coated Si on graphite in type A resulted in reduction of capacity of inner graphite of Si–C composite while the graphite in type B maintained the contact with other particles during charge–discharge. Fig. 8 shows the differential capacity plot of 2nd cycles of types A and B. Li^+ ion intercalates into graphite layers on stage IV, III, II, and I represented by voltage plateaus (peaks A, B, C, D, and E) [22]. In charge, Li^+ ion alloys with Si under 0.3 V while de-alloys over 0.4 V during discharge (peak F). The peak intensities of A, B, C, D, and E of type B are larger than those of type A, and the intensity of peak F is almost equal. This means that the contributing portion of Si is similar in total capacity for both type materials. The different portion of graphite governs the difference of total capacity.

The cycle performance of Si–C composites is shown in Fig. 9. After 30 cycles, the capacity retention rate of types A and B is 78% and 73%, respectively. Better cycling performance of type A can be explained by the difference of Si form in Si–C composite. Si particles are uniformly coated on graphite about 1 μm thickness in type A, while embedded Si particles are non-uniformly aggregated in the graphite in type B. In type B, the volume change of non-uniform Si damages graphite portion in a particle while the graphite portion remains intact in type A.

To verify the difference of degradation, the cross sectional images of pristine electrodes (Fig. 10) were investigated. In type A, there is no signature of damaged particle while inter-particle cleavage is observed. In type B, the damaged graphite portion was observed as well as inter-particle cleavage. The inter-particle cleavage is the common factor of the capacity loss but the damaged graphite portion in particles of type B attributed to the additional loss of capacity.

4. Conclusion

Si powders located in different sites in Si–C composites (type A: surface coated; type B: inner-particle embedded) are successfully synthesized and tested as an anode material for lithium secondary batteries. Electrochemical characterization revealed that the polarization is not increased by Si but the capacity of graphite is decreased in type A. In type B, the damaged graphite by agglomerated Si particles induces the capacity loss during cycles because of losing electrical contact.

Acknowledgement

This work was supported by the division of advanced batteries in NGE program (project No. = 10016453).

Appendix A. Supplementary data

Supplementary data associated with this article can be found, in the online version, at doi:10.1016/j.jpowsour.2010.03.008.

References

[1] J.W. Kim, J.H. Ryu, K.T. Lee, S.M. Oh, J. Power Sources 147 (2005) 227–233.
[2] W.J. Weydanz, M. Wohlfahrt-Mehrens, R.A. Huggins, J. Power Sources 81–82 (1999) 237–242.
[3] B. Gao, S. Sinha, L. Fleming, O. Zhou, Adv. Mater. 13 (2001) 816–819.
[4] J.H. Ryu, J.W. Kim, Y.-E. Sung, S.M. Oh, Electrochem. Solid State Lett. 7 (2004) A306–A309.
[5] U. Kasavajjula, C. Wang, A.J. Appleby, J. Power Sources 163 (2007) 1003–1039.
[6] Z.P. Guo, J.Z. Wang, H.K. Liu, S.X. Dou, J. Power Sources 146 (2005) 448–451.
[7] H. Li, X. Huang, L. Chen, Z. Wu, Y. Liang, Electrochem. Solid State Lett. 2 (1999) 547–549.
[8] I.-S. Kim, P.N. Kumta, G.E. Blomgren, Electrochem. Solid State Lett. 3 (2000) 493–496.
[9] Y. Liu, K. Hanai, T. Matsumura, N. Imanishi, A. Hirano, Y. Takeda, Electrochem. Solid State Lett. 7 (2004) A492–A495.
[10] A. Netz, R.A. Huggins, W. Weppner, J. Power Sources 119–121 (2003) 95–100.
[11] J. Wolfenstine, J. Power Sources 124 (2003) 241–245.
[12] G.X. Wang, L. Sun, D.H. Bradhurst, S. Zhong, S.X. Dou, H.K. Liu, J. Power Sources 88 (2000) 278–281.
[13] J. Yang, Y. Takeda, N. Imanishi, C. Capiglia, J.Y. Xie, O. Yamamoto, Solid State Ionics 152–153 (2002) 125–129.
[14] P. Limthongkul, Y.-I. Jang, N.J. Dudney, Y.-M. Chiang, J. Power Sources 119–121 (2003) 604–609.
[15] K. Yoshimura, J. Suzuki, K. Sekine, T. Takamura, J. Power Sources 146 (2005) 445–447.
[16] J.P. Maranchi, A.F. Hepp, A.G. Evans, N.T. Nuhfer, P.N. Kumta, J. Electrochem. Soc. 153 (2006) A1246–A1253.
[17] M. Uehara, J. Suzuki, K. Tamura, K. Sekine, T. Takamura, J. Power Sources 146 (2005) 441–444.
[18] Y.S. Jung, K.T. Lee, S.M. Oh, Electrochim. Acta 52 (2007) 7061–7067.
[19] V.G. Khomenko, V.Z. Barsukov, J.E. Doninger, I.V. Barsukov, J. Power Sources 165 (2007) 598–608.
[20] L. Chen, X. Xie, A. Wang, K. Wang, J. Xie, Mater. Sci. Eng. B 131 (2006) 186–190.
[21] K. Ohzeki, Y. Saito, B. Golman, K. Shinohara, Carbon 43 (2005) 1673–1679.
[22] M. Wakihara, O. Yamamoto, Lithium Ion Batteries, Wiley-VCH, 1998, pp. 98–126.